Structure of $La_2NiO_{4.18}$

Apurva Mehta and Peter J. Heaney
Princeton Materials Institute and Department of Geological and Geophysical Sciences, Princeton University, Princeton, New Jersey 08544
(Received 24 March 1993)

The published structure of La_2NiO_{4+y} has unusually short (1.94 Å) Ni-O bond lengths. We reexamined the structure of $La_2NiO_{4.18}$ using monochromatic synchrotron x-ray radiation. Rietveld refinement of the structure in space group *Bbcm* yielded Fourier synthesis (F_{obs}) maps that suggest a modified structural model for $La_2NiO_{4.18}$. The refined structure contains chemically more reasonable interatomic distances (e.g., shortest Ni-O distance of 2.00 Å). A comparison of this structure with that of the superconductor La_2CuO_{4+y} reveals disparities in the conduction planes of the two materials that may explain differences in electrical behavior.

INTRODUCTION

Most R_2MO_{4+y} (R = rare earth, M = Cu, Ni, Co, Fe) compounds have technologically useful properties. The cuprates were the first of the high-temperature superconductors, and the electrical properties of the nickelates make them good candidates for high-temperature electrodes. There also is renewed interest in the nickelates because some of the highly acceptor-doped nickelates show traces of superconductivity.[1] Understanding the crystal chemistry of the phases within the R_2MO_4 system is clearly necessary in order to exploit these compounds to their fullest potential, and the development of superior materials depends on a precise determination of the relationship between their crystal structures and their chemical properties.

The La_2MO_4 (M = Cu, Ni, Co, Fe) compounds crystallize in one of the distorted variants of the tetragonal K_2NiF_4 structure (space group: $I4/mmm$). In this paper, the nonstandard space-group setting $F4/mmm$ is used instead of $I4/mmm$ to keep the crystallographic axes oriented similarly throughout. Goodenough and Manthiram[2] have proposed a driving mechanism for the distortion of the ideal tetragonal structure. The La_2MO_4 structure can be viewed as a monolayer epitaxial sandwich of the rocksaltlike La-O layer and the perovskitelike $LaMO_3$ layer. Goodenough and Manthiram propose that if the lattice parameters of the component epitaxial layers match, then the compound crystallizes in the ideal tetragonal K_2NiF_4 structure. However, in all La_2MO_4 (M = Cu, Ni, Co, Fe) compounds the ideal M-O distances are too long to match perfectly the lattice parameters of the ideal rocksalt La-O layers.[3] This interlayer lattice mismatch distorts the ideal tetragonal structure.

The misfit between the two layers can be minimized either by expansion of the La-O layer and/or by compression of the $LaMO_3$ layer. In most perovskites, the octahedral orientation (i.e., the O-M-O angle) is easily varied. Hence, it is presumed that the compression of the perovskite layer would take place predominantly through MO_6 octahedral rotation rather than the contraction of the M-O bond. For example, in the case of La_2CuO_4, most of the mismatch is taken up by the buckling of the CuO_2 planes; this buckling is equivalent to an octahedral rotation about the [100] axis—see Ref. 4. The buckling of the CuO_2 planes lowers the structural symmetry to orthorhombic with space group *Bmab* (again, a nonstandard space-group setting is used to keep the axes orientation consistent with $F4/mmm$). Therefore, the degree of orthorhombicity can be used as a measure of the rotational distortion in the perovskite layer.

Nickel has a larger ionic radius than copper, and hence by analogy to the cuprate, one would expect a greater amount of octahedral rotation (and thus orthorhombicity) in the nickelate. However, the degree of orthorhombicity (and thus the amount of octahedral rotation) for the published structure of La_2NiO_4 (Refs. 5 and 6) is comparable to that for La_2CuO_4.[7] Thus, the published structural model seems to imply that a large fraction of the perovskite layer compression in La_2NiO_4 is accomplished by the contraction of Ni-O bonds. Some of the Ni-O bonds in the reported structure of La_2NiO_4 are severely contracted (1.95 Å compared to 2.09 Å in NiO). Hence, if the reported structure of La_2NiO_4 is accurate, then it would seem that some crystallographic constraint inhibits the buckling of the NiO_2 layer, which is usually pliable.

The expansion of the rocksalt layer, aside from stretching the La-O bond, can take place by insertion of extra atoms in that layer. It is believed that the excess oxygen in La_2NiO_{4+y} goes in the La-O rocksalt layer.[5] The expanded La-O layer, however, is still too compact to match the undistorted $LaNiO_3$ perovskite layer. The NiO_6 octahedra in the reported structure of $La_2NiO_{4.18}$ are only slightly rotated from the ideal perovskite orientation, and, surprisingly, the $LaNiO_3$ perovskite layer contracts through the shortening of Ni-O bonds.[5] As a result, the Ni-O bonds in $La_2NiO_{4.18}$ are even shorter than they are in La_2NiO_4 [1.93 Å (Ref. 5) compared to 1.95 Å (Refs. 5 and 6)]. If the reported structures of La_2NiO_{4+y} ($y > 0$) are accurate, then these compounds

contain the shortest known Ni^{+2}-O bonds. This has profound significance for the study of the electrical properties of these compounds, as the Fermi surface in these materials is predominantly determined by the transition-metal-oxygen interactions.

In this paper, we reexamine the structure of $La_2NiO_{4.18}$ using monochromatic synchrotron radiation. The extremely narrow line shape of the synchrotron source makes it ideal for direct observation of the cell symmetry. Based on the interpretation of Fourier synthesis maps generated during the refinement procedure using Rietveld methods, we propose an alternative structural model for $La_2NiO_{4.18}$ that yields chemically more reasonable interatomic distances. Comparison of our derived structure of La_2NiO_{4+y} with La_2CuO_{4+y} sheds light on the nature of the basal plane in the two structures.

EXPERIMENT

Stoichiometric amounts of La_2O_3 (Aesar 99.99%; dried at 973 K prior to use) and NiO (Aesar 99.999%) were ground in an agate mortar and heated in a platinum crucible at 1373 K for 12 h. The calcined powder was then well ground and heated at 1523 K for 24 h, annealed at 973 K in air for 24 h, and quenched to room temperature (295 K).

The oxygen stoichiometry was determined by a programmed temperature reduction cycle using a Cahn 113 thermal balance system (at Brown University). About 100 mg of the sample was loaded in a thermogravimetric analysis bucket and the system was purged at room temperature in a stream of 15% H_2 in Ar until a constant weight was reached. The flow rate of the gas mixture was maintained at 50 sccm. The temperature was then increased to 1173 K at a rate of 200 K/h and held at 1173 K for 1 h. The reduction products were determined from x-ray analysis to be Ni metal and La oxide. The oxygen stoichiometry of the sample was determined to be 4.18(1) (i.e., $La_2NiO_{4.18}$) from the weight loss on reduction.

Initial diffraction experiments were performed with a Scintag PAD V automated diffractometer with Cu $K\alpha$ radiation to determine the phase purity of the sample. Diffraction results indicated that $La_2NiO_{4.18}$ was phase pure. Powder x-ray-diffraction data for structure refinement were collected using monochromatic synchrotron radiation at beam line X7A, at the National Synchrotron Light Source, Brookhaven National Lab. The x-ray wavelength was determined to be 1.1497 Å using a silicon standard. The data were collected in Bragg-Bretano geometry using a diffractometer with an incident beam and reflected beam (Ge111 and Ge220) monochromator. The diffraction pattern was collected from 10° to 80° 2θ (6.6–0.9 Å) at every 0.005° 2θ with counting time of 3 sec per step. Trace amounts of NiO were detected in the diffraction data collected using the synchrotron radiation.

Structure refinement was performed using the Rietveld method [program GSAS (Ref. 8)]. The background was fitted using five refinable coefficients in a cosine Fourier series. Multiterm (eight terms: four Gaussians, two Lorentzians, sample displacement, and sample transparency) Simpson's rule integration of the symmetric pseudo-Voigt profile shape functions[8,9] was used to model the Bragg peaks. Initially, the refinement was performed by ignoring the excess oxygen and placing the remaining atoms in the positions refined by Jorgensen *et al.*[5] in the *Fmmm* symmetry as starting positions. The atoms were assigned isotropic temperature factors. After refinement, observed Fourier (F_{obs}) maps were generated and the excess oxygens were introduced into the *Fmmm* structure at the positions indicated by concentrated electron density in the F_{obs} maps. At this point, the positions and the occupancies of the excess oxygen atoms and the occupancy of the apical oxygen were refined, with all other parameters fixed. We were unable to refine the occupancy of the oxygen sites in the full structural refinement due to severe correlation effects. We next attempted a refinement of the position of the basal oxygen by lifting the constraint on its position in the basal plane [new site at $(x,y,0)$] in the space group *Bbcm* (nonstandard space-group setting used to keep the axes orientation consistent with *F4/mmm*). The residual improved only marginally. In addition, attempts to refine the structure in a space group other than orthorhombic (for instance, monoclinic space group *B2*) did not significantly improve the refinement results.

RESULTS AND DISCUSSION

Departures from tetragonal symmetry

To our knowledge, none of the published neutron- and x-ray-diffraction studies on La_2NiO_{4+y} ($y \sim 0.18$) have revealed peak splitting indicative of a lattice symmetry lower than tetragonal. However, electron-diffraction studies show superlattice spots indicative of an orthorhombic lattice,[10] and Jorgensen *et al.*[5] refined the structure of $La_2NiO_{4.18}$ from neutron-diffraction data in an orthorhombic space group (*Fmmm* and *Bmab*) assuming a systematic broadening of Bragg peaks.

All the observed Bragg peaks obtained on our Scintag PAD V diffractometer could be indexed with the tetragonal (*F4/mmm*) K_2NiF_4 cell. However, a careful observation of the (400) peak using synchrotron radiation (see

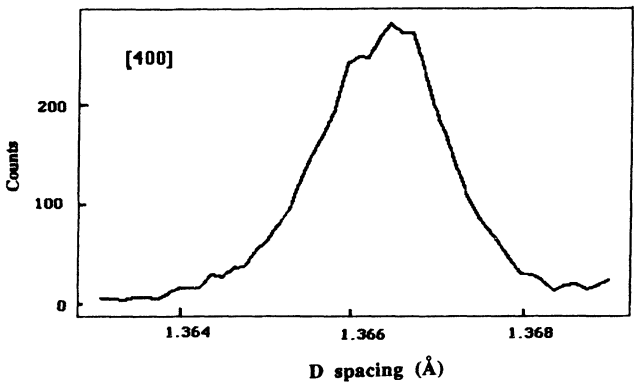

FIG. 1. The (400) Bragg peak of $La_2NiO_{4.18}$ reveals peak splitting due to orthorhombicity.

Fig. 1) indicates that the peak is a doublet and the lattice symmetry is no higher than orthorhombic. The doublet spacing corresponds to a difference in length between the **a** and **b** axes of no more than 0.005 Å. Jorgensen *et al.*[5] using neutron radiation obtained a larger difference between the **a** and **b** axes for a chemically identical sample.

The orthorhombic subgroup of *F4/mmm* with the highest symmetry is *Fmmm*. Thus, the initial structural model for our refinement of $La_2NiO_{4.18}$ was chosen to be *Fmmm*. The parameters refined via the Rietveld method for *Fmmm* and *Bbcm* symmetry are listed in Table I. The raw data, the calculated profile, and the difference curve for the *Fmmm* and *Bbcm* refinement are plotted in Fig. 2. The refined parameters for $La_2NiO_{4.18}$ in the *Fmmm* symmetry reported here are similar to those obtained by Jorgensen *et al.*,[5] based on the analysis of powder neutron-diffraction measurements, for a chemically identical sample (see Table I). Although the two sets of data differ by more than the estimated standard deviation (ESD), it is likely that the ESD's are underestimated by the Rietveld refinement method.

Octahedral Rotations and Microtwins

An observed Fourier (F_{obs}) map representing the basal (001) section of the refined *Fmmm* structure is shown in Fig. 3. The electron-density concentration at the center of the map [(000) position] corresponds to nickel. However, the electron-density contours suggest that the basal oxygen site at $(\frac{1}{4},\frac{1}{4},0)$ is split. We propose that the positionally split O_{basal} site is indicative of the rotation of the

TABLE I. Refined structural parameters for $La_2NiO_{4.18}$ at 295 K. Numbers in the parentheses are the estimated standard deviation of the last significant digit. $\chi^2=(R_{wp}/R_{exp})^2$ where R_{wp} is the residual obtained using intensity weighting (see Ref. 8 for details).

	Fmmm (This work)	*Bbcm* (This work)	*Fmmm* (Ref. 5)
a	5.46520(7) Å	5.46520(7) Å	5.4614(2) Å
b	5.46869(7) Å	5.46869(7) Å	5.4723(2) Å
c	12.67804(15) Å	12.67804(15) Å	12.7138(2) Å
La	$x=y=0$	$x=y=0$	$x=y=0$
	$z=0.36117(4)$	$z=0.36117(4)$	$z=0.3600(1)$
	$B(Å^2)=0.12(1)$	$B(Å^2)=0.12(1)$	$B(Å^2)=0.44(3)$
Ni	$x=y=z=0$	$x=y=z=0$	$x=y=z=0$
	$B(Å^2)=0.24(3)$	$B(Å^2)=0.24(3)$	$B(Å^2)=0.30(3)$
O_{apical}	$x=y=0$	$x=y=0$	$x=y=0$
	$z=0.1775(4)$	$z=0.1775(4)$	$z=0.1733(5)$
	$B(Å^2)=2.1(1)$	$B(Å^2)=2.1(1)$	$B(Å^2)=0.7(1)$
O_{basal}	$z=0$	$z=0$	$z=0$
	$x=y=0.25$	$x=0.254(9)$	$x=y=0.25$
		$y=0.25(1)$	
	$B(Å^2)=0.2(1)$	$B(Å^2)=0.2(1)$	$B(A^2)=0.27(3)$
R_{exp}	13.77%	13.77%	4.89%
χ^2	1.987	1.988	2.640

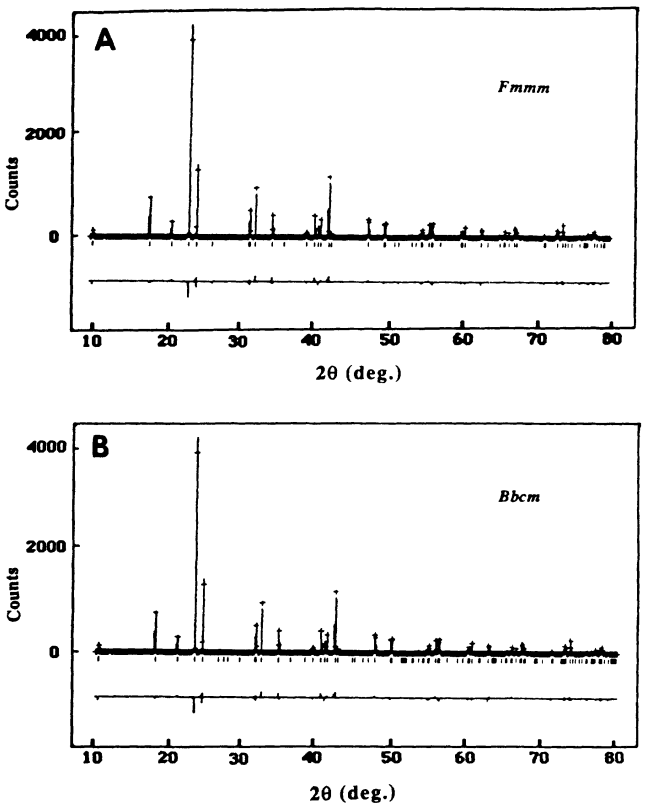

FIG. 2. The Rietveld refinement profiles for the (a) *Fmmm* and (b) *Bbcm* structure of $La_2NiO_{4.18}$ at 295 K. The plus marks are the raw data points and the solid curve is the calculated profile. The difference between the two (observed—calculated) is plotted at the bottom of each figure. The tick marks below the profiles indicate the positions of the allowed reflections.

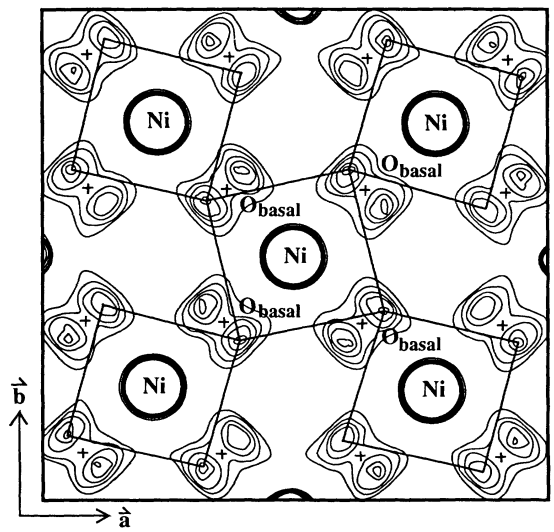

FIG. 3. An observed Fourier synthesis (F_{obs}) map showing the basal (001) section of the structure of $La_2NiO_{4.18}$. Splitting of the basal oxygen positions suggests that octahedra are rotated about **c** on a local scale. The octahedra corresponding to the *l* twin configuration are outlined.

NiO_6 octahedron about the c axis. The central NiO_6 octahedron with Ni at (000) can rotate either clockwise (d) or counterclockwise (l). In Fig. 3, the octahedra corresponding to the l rotation are outlined. The two possible rotations, d and l, give rise to two sets of twins that are related by mirror planes along {110}. This octahedral rotation is different from (and orthogonal to) the rotation that causes the buckling of the basal plane and gives rise to *Bmab* cell symmetry. The F_{obs} map of the section perpendicular to the basal plane and passing through the basal oxygen doublet indicates no significant displacement of the oxygen from the basal plane (Fig. 4). This suggests that the octahedra are rotated primarily about the c axis. The c-axis octahedral rotation lowers the symmetry of the unit cell from *Fmmm* to *Bbcm*, which is a proper subgroup of *Fmmm*. Thus, the F_{obs} map generated from the *Fmmm* symmetry represents the superposition of the two twin configurations.

During the structure refinement in space group *Bbcm*, the basal oxygen moved slightly away from the special position with $2/m$ symmetry. However, the new refined position of the basal oxygen at [0.254(9), 0.249(13), 0] (see Table I) is significantly distant from the closest electron-density concentration at (0.183, 0.317, 0) as seen in the F_{obs} map (Fig. 3). X-ray- and neutron-diffraction data represent the spatial average of a crystal structure over a correlation length of a few hundred Å. Hence, if the l and the d *Bbcm* twins in the sample are smaller than the correlation length, then the Rietveld analysis will converge to the spatial average of the two twin sets (see the Appendix for details). The existence of small l and d twin domains could account for the discrepancy between the positions of the basal oxygen atoms refined during Rietveld analysis and those indicated by the F_{obs} maps.

Rodriguez-Carvajal, Fernandez-Diaz, and Martinez[6] also observe that x-ray diffraction cannot resolve microstructural features of $La_2NiO_{4.18}$ at a nanometric scale. However, Rodriguez-Carvajal, Fernandez-Diaz, and Martinez note that fine-scale twinning will broaden x-ray-diffraction peaks anisotropically, and such anisotropic broadening of peaks can be seen in our data (see Fig. 5). High-resolution transmission-electron microscopy (HREM) is best suited to the investigation of microstructural twins, and we hope to complete such an investigation in the near future.

When a material undergoes a phase transition that alters its unit-cell parameters anisotropically, the resultant strain is usually relieved by twinning. The twin size in a material is, therefore, determined by a balance between the energy gained by relieving the anisotropic strain and the energy required to form a twin boundary. $La_2NiO_{4.18}$ undergoes a phase transition (presumably from $F4/mmm$ to *Fmmm* to *Bbcm*) on cooling from the synthesis tem-

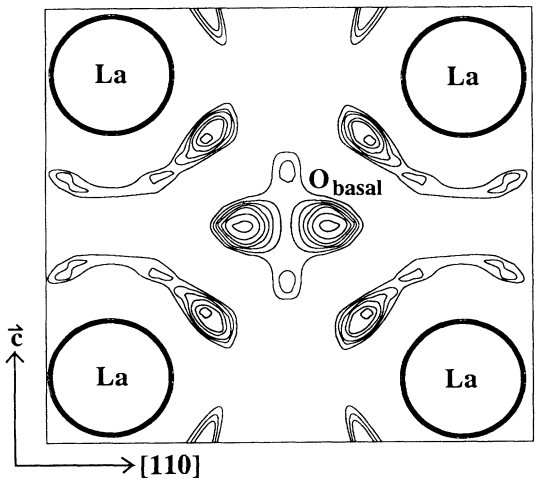

FIG. 4. An observed Fourier synthesis (F_{obs}) map of the ($1\bar{1}0$) section of the $La_2NiO_{4.18}$ structure 2.02 Å above the origin. This section passes through the electron-density maxima of the basal oxygen pairs. Electron density of the basal oxygens is concentrated within the (001) plane. Rings of electron density around La cations are due to termination errors associated with the Fourier synthesis.

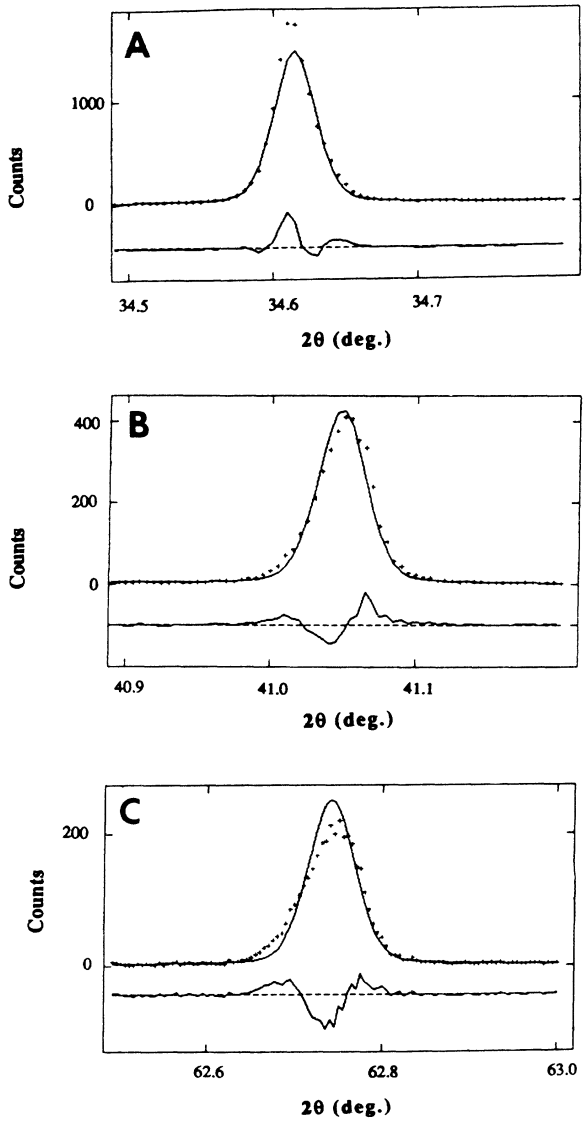

FIG. 5. Enlarged views of anisotropically broadened peaks: (a) (2 2 0); (b) (1 1 7); (c) (1 1.11).

perature, and twins form in order to relieve anisotropic strain. The twin boundaries themselves must have the symmetry of the high-temperature phase. Therefore, the energy to form a twin boundary is a measure of the metastability of the high symmetry phase. The small twin size predicted for the *Bbcm* twin in $La_2NiO_{4.18}$ would imply that the twin boundary energy is low, and thus the high-temperature ($F4/mmm$) structure is not very metastable with respect to the quenched local structure.

Positional disorder among apical oxygens

Figure 6(a) is a section of the F_{obs} map parallel to the basal plane and passing through the apical oxygens at $z = 0.1775$, and Fig. 6(b) is an enlargement showing only the apical oxygen. The map plane also passes through a layer of La atoms; thus, the map shows a section of the La-O rocksalt layer. The electron-density contours at the apical oxygen site in Fig. 6 indicate that electron density is toroidal rather than spherical. We interpret this as evidence for positional disorder at the apical oxygen site. In the structural refinement of Jorgensen *et al.*,[5] a certain fraction of the apical oxygens (the apical oxygens adjacent to the excess interstitial oxygens) are placed very near the toroidal position. They believe that the apical oxygen distorts to accommodate the interstitial oxygen defect, and hence the occupancy of the "distorted" site is coupled to the excess oxygen concentration.

By contrast, we suggest that *all* the apical oxygens belong to the toroidal sites. The apical oxygen may be dynamically disordered within the torus, or they may be localized at certain positions in the torus. The electron-density concentration shown in Fig. 6(b) indicates that the apical oxygens are displaced along the [010] and the [100] directions. If the oxygen atoms occupy one of these toroidal sites, one of the La-O distances is reduced from the normally stretched configuration (at the expense of increasing the other La-O distances). The resultant La-O bond relaxation could be a probable driving mechanism for the toroidal distortion. The placement of oxygen in the toroidal site breaks the twofold rotational symmetry about the c axis and reduces the unit-cell symmetry to monoclinic at a local scale.

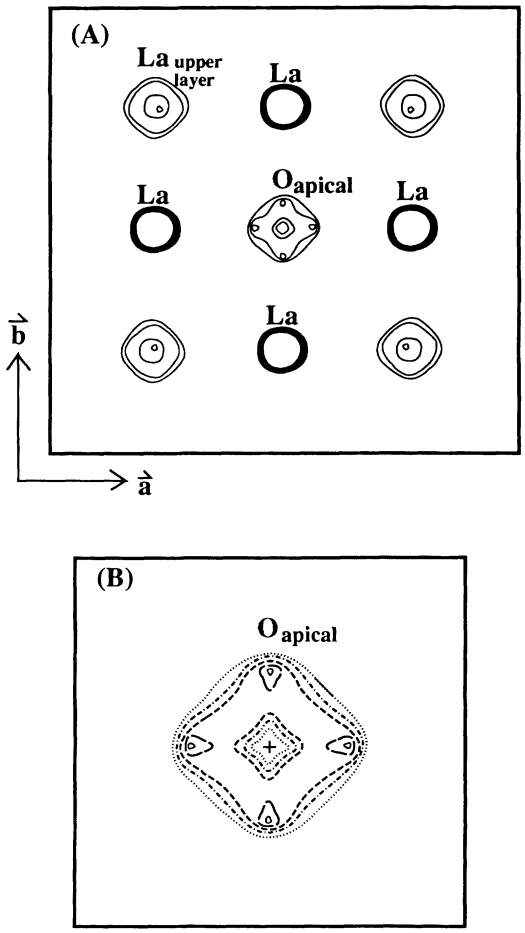

FIG. 6. (a) An observed Fourier synthesis (F_{obs}) map showing a section of the $La_2NiO_{4.18}$ structure parallel to the basal (001) plane and passing through the apical oxygen. Areas of weak electron density correspond to La cations in the layer above this section. (b) An enlarged view of the apical oxygen reveals the toroidal distribution of electron density maxima. The cross marks the refined position for O_{apical}.

Interstitial oxygen atoms

The $(1\bar{1}0)$ section of the F_{obs} map passing through the NiO_6 octahedra (Fig. 7) shows another view of the toroidal nature of the apical oxygen site. The map also shows electron density concentrations at (0.183, 0.183, 0.217) and (0.317, 0.317, 0.217) (marked as O_{excess} on the map), which we attribute to the excess oxygen in the structure. The distance between these two excess oxygen positions is only 1.04 Å, which is too short for nonbonded oxygens. Hence, we suggest that on a local scale only one of these positions is occupied. The *Fmmm* symmetry generates additional excess oxygen positions at (0.183, 0.317, 0.283) and (0.317, 0.183, 0.283); these positions are

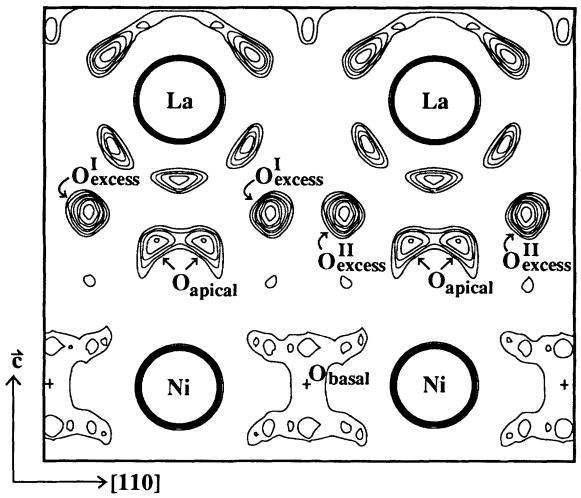

FIG. 7. An observed Fourier synthesis (F_{obs}) map showing the $(1\bar{1}0)$ section of the structure of $La_2NiO_{4.18}$ passing through the NiO_6 octahedra. The splitting of the apical oxygen position is evident, and areas of concentrated electron density reveal excess oxygen positions O^{I} and O^{II}. Annular electron density surrounding La arises from Fourier series termination errors.

not visible in Fig. 7 as they lie in a plane perpendicular to the map plane. These four excess oxygen positions form an elongated tetrahedron. The excess oxygen position refined by Jorgensen *et al.*[5] is at (0.25, 0.25, 0.23). There is no observable electron density at that position in the F_{obs} maps. However, the excess oxygen position postulated by Jorgensen *et al.* is very close to the centroid of the elongated tetrahedron formed by the four electron-density concentrations attributed to the excess oxygens in our F_{obs} maps. Again, this discrepancy between the local electron-density concentration and the oxygen position refined using the Rietveld method could arise from the use of integrated Bragg intensities that spatially average the local structure over the x-ray correlation length (see the Appendix for details).

The excess oxygen position indicated by the electron-density concentration is also unusually close to the apical oxygen site (O-O distance of 1.41 Å). Jorgensen *et al.* suggest that the apical oxygen adjacent to the excess oxygen is displaced from the c axis to $(-0.060, -0.069, 0.172)$; this increases the O-O distance to 1.95 Å. However, this distance is still unusually short for nonbonded oxygens. We suggest that when one of the excess oxygen sites is occupied, then the excess oxygen related to it by a twofold rotation about the c axis also is occupied, but the adjacent apical oxygen site is vacant. This model leads to two possible pair configurations for excess oxygen, and they are depicted as O^{I}_{excess} and O^{II}_{excess} in Fig. 7.

The advantage of this model is that each excess oxygen anion is separated from the nearest oxygen anion (the other excess oxygen) by a distance of 2.83 Å, which is close to the minimum permissible distance for a nonbonded oxygen pair. Thus, the incorporation of the excess oxygen in $La_2NiO_{4.18}$ is modeled as a substitution of a nonbonded O^{I}-O^{I} pair (or an O^{II}-O^{II} pair) for an apical oxygen. Occupancy of every two "interstitial" oxygen sites creates one "vacancy" at the apical site. After refinement of the occupancies of the oxygen sites (with all other parameters fixed), the oxygen excess site had a 35–40% occupancy, whereas the apical oxygen site displayed a 20% vacancy. Therefore, the refinement results strongly support the proposed oxygen excess incorporation model.

Defect analysis of excess and apical oxygen atoms

The oxygen Frenkel defect reaction, given below in the Kröger-Vink notation:[11]

$$O_O + V_I \longrightarrow V_O^{00} + O_I^{ll} \quad (1)$$

shows an interrelationship between the oxygen vacancy and the oxygen interstitial. In the absence of strong defect interactions, the mass action law can be applied to the Frenkel reaction yielding the following mathematical relationship between the two types of oxygen defects:

$$[V_O^{00}][O_I^{ll}] = K_{OF}(T) , \quad (2)$$

where K_{OF} is the oxygen Frenkel constant. In the realm of noninteracting defect chemistry K_{OF} is a function only of temperature. Thus, at a given temperature the product of the concentration of oxygen vacancies and interstitials is a constant. Though the two defects do not interact with each other, their concentrations (over the whole structure) are related through the mass action law; the oxygen interstitial concentration varies inversely as the oxygen vacancy concentration. However, in the oxygen excess defect configuration proposed in this paper (or for that matter in the defect configuration proposed by Jorgensen *et al.*), the oxygen interstitial concentration (i.e., the concentration of the site for the excess oxygen) and the oxygen vacancy concentration (i.e., the concentration of the empty apical oxygen sites) are coupled on a *local* scale. Chemical considerations dictate that the two defect concentrations are *directly* proportional to each other rather than through the inverse relationship suggested by the mass action law and would, thus, violate the mass action law. Therefore, the proposed oxygen excess configuration cannot be treated as point defects in La_2NiO_4 from the perspective of dilute solution defect chemistry.

However, it is possible to apply dilute solution defect chemistry if the notions of oxygen interstitials and oxygen vacancies in $La_2NiO_{4.18}$ are redefined. For this purpose, the excess interstitial oxygen pair (O^{I}-O^{I} or O^{II}-O^{II}) can be conceived as a single unit substituting for the oxygen at the apical site. In this perspective, the "defect complex" is a crystallographically unique site in the lattice and hence the interstitial oxygens and the vacant apical site (forming the complex) are not *defects* but normal parts of the structure of $La_2NiO_{4.18}$ and thus need not obey the mass action law for oxygen defects. In the redefined structure, there are *two* crystallographically unique apical octahedral sites, as opposed to La_2NiO_4 in which there is only one unique apical octahedral site.

Therefore, the oxygen excess incorporation mechanism proposed in this paper results in a crystallographically and thermodynamically different phase from La_2NiO_4. It is possible that the excess oxygens in La_2NiO_{4+y} for small y do not strongly interact with each other or with the rest of the parent structure and thus are incorporated in the structure in a conventional way forming oxygen interstitial defects. However, with increasing concentration of excess oxygen, the interstitial defects are close enough to interact strongly with each other. The mode of oxygen excess incorporation could change to the one proposed in this paper and the material transforms to a new phase. It has been shown that La_2NiO_{4+y} exhibits two-phase behavior in the range $0.02 < y < 0.13$.[12] We speculate that this phase transition is driven by the strong interactions of oxygen interstitials and reflects a change in the oxygen excess incorporation mechanism.

The two types of apical octahedral sites (i.e., the normal site and the site modified by the excess oxygens) in $La_2NiO_{4.18}$ could order to form a superstructure. If, for example, $\frac{1}{4}$ of the apical sties are modified, then the smallest superperiodic cell has four times the volume of the "standard" cell (5.46 Å × 5.46 Å × 12.67 Å) and the oxygen stoichiometry of the material is 4.25 (i.e., $y = 0.25$ in La_2NiO_{4+y}). In general, for the oxygen stoichiometry of $4+y$ the volume of the smallest superperiodic cell is

$1/y$ the volume of the standard cell. Brown has suggested one such superstructure (*Ibam*: $2a \times 3b \times c$) for $La_2NiO_{4.16}$;[13] however, even on careful examination of the low angle synchrotron data we could not detect any peaks consistent with the superstructure proposed by Brown. It is possible that either the material is not (fully) ordered at room temperature or that the material is ordered into a series of superstructures (e.g., for $La_2NiO_{4.25}$ some of the possibilities are $2a \times 2b \times c$, $4a \times b \times c$, $a \times b \times 4c$, etc.) with only short-range coherence (and perhaps even slightly different oxygen stoichiometry). However, powder diffraction is not the most sensitive technique for the investigation of such microstructures, and no attempts were made to include possible superstructures in the structural refinement procedures. On the other hand, high-resolution transmission-electron microscopy (HREM) is very well suited to such observations.

CONDUCTION GEOMETRY IN La_2NiO_{4+y} AND La_2CuO_{4+y}

The crystal structures of the nickelates and the cuprates are very similar to each other; however, the small differences between the two structures are of paramount importance because they suggest a crystallographic basis for the differences in their properties.

If one looks at the geometry of the CuO_6 octahedral layer in La_2CuO_{4+y}, it is evident that the axial Cu-O bonds (the bonds along the **c** axis) are much longer than the basal Cu-O bonds [2.43 vs 1.90 Å (Ref. 14)]. On the other hand, the Ni-O bond lengths in the NiO_6 octahedron in $La_2NiO_{4.18}$ are similar to each other (2.28 vs 2.00 Å—see Table II). Based on the extremely long axial Cu-O bond lengths, the apical oxygens are thought to be weakly bound to the copper cations, and the CuO_6 octahedral layer is, thus, reduced to a two-dimensional plane composed of a copper and the two basal oxygens. It is widely believed that these two-dimensional conduction planes are essential for superconductivity. However, the apical oxygen-nickel bond lengths in La_2NiO_{4+y} are comparable to the basal oxygen-nickel bond lengths, and thus the apical oxygens are almost as strongly bonded to the nickel as are the basal oxygens, and consequently it is unlikely that the structure contains two-dimensional NiO_2 basal planes.

Another and perhaps stronger argument concerning the lack of NiO_2 two-dimensional (2D) conduction planes in La_2NiO_{4+y} is based on the determination of the ionic radius of the nickel and the copper ion from *M*-O (*M* = Cu, Ni) bond lengths. As the three *M*-O (*M* = Cu, Ni) bond lengths are not equal, there are three different effective ionic radii for the Cu/Ni ion along three orthogonal directions. In La_2CuO_{4+y}, copper has an ionic radius of 1.03 Å along the **c** axis and 0.50 Å along the **a** and **b** axes (oxygen is assumed to have an ionic radius of 1.40 Å (Ref. 14)]. An ionic radius of 1.03 Å is much too large for any valence of copper in any possible coordination geometry;[14] however, the ionic radius of 0.50 Å is close to the average ionic radius of Cu^{+2} in square planar coordination (0.57 Å).[14] Therefore, one may conclude that copper in La_2CuO_{4+y} is in square planar coordination, essentially forming two-dimensional CuO_2 planes. [Note: the ionic radius of Cu^{+2} in octahedral coordination is 0.73 Å (Ref. 14).] On the other hand, the ionic radius of nickel in La_2NiO_{4+y} along the **a** and **b** axes is 0.60 Å. This radius best matches the ionic radius of nickel in octahedral coordination [Ni^{+2}=0.69 Å, Ni^{+3} (low spin) =0.56 Å, Ni^{+3} (high spin) = 0.60 Å (Ref. 14)]. Therefore, the apical oxygen-nickel bond in La_2NiO_{4+y} cannot be neglected, so that a 2D NiO_2 conduction plane cannot be isolated from the NiO_6 octahedral layer.

TABLE II. Atom positions and interatomic distances in $La_2NiO_{4.18}$.

Atom type	Position[a]		
	x	*y*	*z*
Ni	0	0	0
La	0	0	0.3612
O_{apical} (occupancy=82%)	0	0.074	0.1775
O_{basal}	0.317	0.183	0
O_{excess}[b] (occupancy=36%)	0.183	0.183	0
Ni-O_{basal}[c]	(4)2.00(1) Å		
Ni-O_{apical}	(1.64)2.28(1) Å		
La-O_{basal}	(4)2.26(2) Å	(4)3.02(2) Å	
La-O_{apical}	(1.64)2.36(1) Å	(1.64)2.38(1) Å	
	(1.64)3.18(1) Å	(3.38)2.81(1) Å	
Ni-O_{excess}	(0.36)3.09(2) Å	(0.36)3.68(2) Å	
	(0.72)4.11(2) Å		
La-O_{excess}	(0.36)2.31(1) Å	(0.36)3.06(1) Å	
	(0.36)2.23(1) Å		
O_{basal}-O_{basal}	(4)2.83(1) Å		
O_{basal}-O_{apical}	(3.38)2.80(1) Å	(3.38)3.62(2) Å	
O_{excess}-O_{excess}[b]	(0.18)2.83(2) Å		
O_{basal}-O_{excess}	(0.36)2.84(2) Å		

[a]The atom positions are given with respect to the *F4/mmm* structure. Symmetry-related positions are not listed.
[b]Refer to the text for the sites of the excess oxygen defects.
[c]Number in the parentheses before the bond length refers to the number of bonds per formula unit. In calculating the bond lengths the small amount of orthorhombicity (<0.1%) is ignored. The number in the parenthesis after the bond length is the estimated standard deviation of the last significant digit.

ACKNOWLEDGMENTS

We would like to thank J. DiCarlo of Princeton University for his help in sample synthesis and oxygen stoichiometry determination, A. Wold of Brown University for the use of his thermogravimetric system, A. Koen and J. Pluth of University of Chicago, and D. E. Cox of Brookhaven National Laboratory for their help in collecting the synchrotron data. We also thank J. DiCarlo and A. Navrotsky of Princeton University, J. Post of Smithsonian Institute, D. Bish and R. Von Dreele of Los Alamos National Laboratory, and I. D. Brown of McMaster University for insightful discussions. The work was supported by National Science Foundation (Grant No. DMR-89-12549 and EAR-92-06031) and the Center for High Pressure Research, an NSF science and technology center.

APPENDIX

The width of a Bragg peak ($\Delta\theta$), defined as the angular distance between the zeros on either side of the principal maximum, in a diffraction grating spectrum from incoherent monochromatic radiation is given by[15]

$$\Delta\theta = 2\lambda/(Na\cos\theta_b)\ , \tag{A1}$$

where θ_b is the angular position of the Bragg peak, λ is the wavelength of the radiation, a is the spacing of the grating, and N is the size of the grating. In diffraction from a crystal lattice, N is the number of unit cells contributing towards the diffraction peak, and thus, Na is usually the crystal size. (It is the average crystallite size in powder diffraction and the average twin size for a twinned material.)

On the other hand, the angular separation of the Bragg maxima ($\Delta\theta_b$) of the same order for two gratings with slightly different spacings can be obtained by differentiation of Laue's equation:[15]

$$a\sin\theta_b = n\lambda \tag{A2a}$$

and is given by

$$\Delta\theta_b = (\Delta a/a)\tan\theta_b\ , \tag{A2b}$$

where θ_b is the average angular position of the Bragg maxima, n is the order of the Bragg reflection, and a is the average grating spacing. A "Bragg peak doublet" from a powdered or a twinned material with two an different lattice parameters (say, an orthorhombic lattice with a small difference in the **a** and the **b** axes) can be analyzed similarly. If the separation between the two Bragg peaks within a doublet $\Delta\theta_b$ is much larger than the width $\Delta\theta$ of the individual peaks, then the difference between the **a** and the **b** axes and hence the orthorhombic symmetry of the lattice will be well resolved in the diffraction measurement. If, however, the peaks are broader than the separation between them, then they would merge into a broad composite peak and the orthorhombic symmetry of the lattice will be lost in diffraction. This resolution criterion can be represented by the following inequality:

$$\Delta\theta_b \geq \Delta\theta, \quad \text{or } (\Delta a/a)\tan\theta_b \geq 2\lambda/(Na\cos\theta_b) \tag{A3}$$

and thus,

$$Na \geq 2\lambda/[(\Delta a/a)\sin\theta_b] = L\{\theta_b, \lambda, (\Delta a/a)\}\ . \tag{A3a}$$

The right-hand side of Eq. (A3a) defines L, the correlation length. The resolution criterion can be restated as follows. The full lattice symmetry is visible in powder diffraction if the crystallite (or the twin) size is larger than the correlation length. Hence, the smaller the correlation length, the more sensitive a diffraction measurement is to the local lattice symmetry. Therefore, the smaller wavelength of a high-energy ($\sim$100 kV) electron beam produces a much shorter correlation length (only a fraction of the correlation length for a typical x-ray or neutron-diffraction measurement), making high-energy electron diffraction very sensitive to symmetry changes on a local scale. Equation (A3a) also suggests that higher angle diffraction peaks are more sensitive to changes in lattice symmetry.

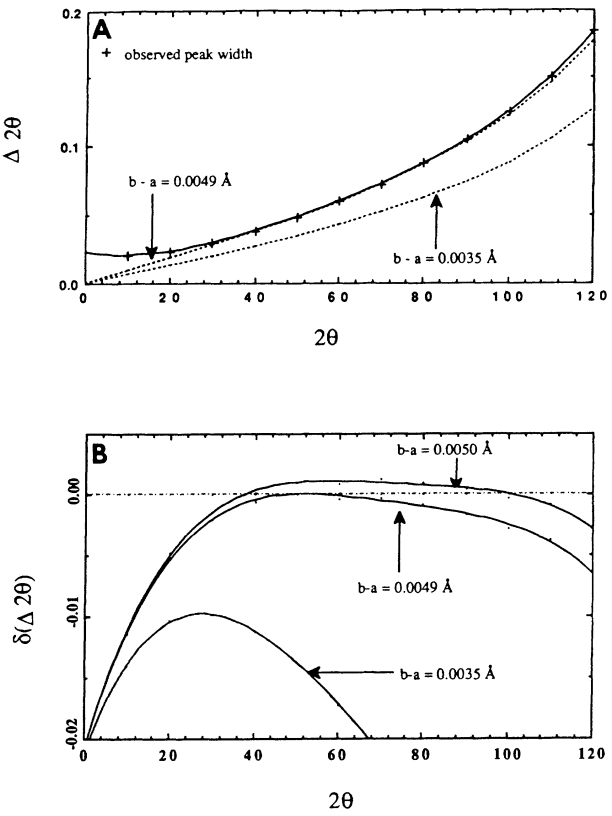

FIG. 8. (a) The measured peak widths in degrees (solid curve) and the separation of the Bragg doublets (dashed curves) as a function of the scattering angle 2θ in degrees. (b) The difference between the Bragg doublet separation and the measured peak widths (in degrees) as a function of the scattering angle 2θ (in deg).

However, in an actual diffraction measurement, other factors contribute to the width of a Bragg peak, such as strain and instrumental parameters. Also, in the previous analysis, the width of a Bragg peak is defined as the angular separation between the first minima on either side of the Bragg maxima; however, in an x-ray-diffraction pattern, the minima are obscured by background. Therefore, the width of the Bragg peak is usually measured as the angular separation between the points at half the maximum intensity; this quantity is known as full width at half maximum (FWHM).

Figure 8(a) shows the observed peak width (FWHM) for $La_2NiO_{4.18}$ as a function of the Bragg angle ($2\theta_b$). The figure also plots a series of curves showing the separation of the orthorhombic doublets, based on Eq. (2), for a small orthorhombicity (**b**$-$**a**) and fixed average basal plane lattice parameters ([**a**+**b**]/2=5.46 Å). For very small orthorhombicity (e.g., **b**$-$**a**=0.0035 Å), the separation of the orthorhombic doublet is less than the width of the peaks at all angles, and hence the (full) orthorhombic symmetry of the lattice would not be discernible. However, for a higher orthorhombicity (**b**$-$**a** $\geq$0.0049

Å) the orthorhombic doublets are separated by more than the width of the peaks for at least a portion of the diffraction pattern, and hence the diffraction pattern is sensitive to the full orthorhombic symmetry of the lattice. In Fig. 8(b), the difference between the peak width and the peak separation [$\delta(\Delta 2\theta)$] is plotted to highlight the crossover. [A positive difference in $\delta(\Delta 2\theta)$ means that the peak separation is larger than the peak width.] It is interesting to note that for a certain range of orthorhombicity (for example, $\mathbf{b}-\mathbf{a}=0.0050$ Å), the high angle diffraction are less sensitive to the full lattice symmetry than the data at intermediate values for 2θ.

[1]K. S. Nanjundaswamy, A. Lewicki, Z. Kakol, P. Gopalan, P. Metcalf, J. M. Honig, C. N. R. Rao, and J. Spalek, Physica C **166**, 361 (1990).

[2]J. B. Goodenough and A. Manthiram, J. Solid State Chem. **88**, 115 (1990).

[3]The structure of CuO and NiO in H. E. Swanson and E. Tatge, Natl. Bur. Stand. (U.S.), Circ. **539**, 49 (1953); the structure of CoO in Natl. Bur. Stand. (U.S.), Circ. **539**, 28 (1960); the structure of Fe_2O_3 in Natl. Bur. Stand. (U.S.), Monogr. **25**, 18 (1981); the structure of La_2O_3 in H. E. Swanson and R. K. Fuyat, Natl. Bur. Stand. (U.S.), Circ. **539**, 33 (1954); also see Ref. 14.

[4]Y. Maeno, A. Odagawa, N. Kakehi, T. Suzuki, and T. Fujita, Physica C **173**, 322 (1991).

[5]J. D. Jorgensen, B. Dabrowski, S. Pei, D. R. Richards, and D. G. Hinks, Phys. Rev. B **40**, 2187 (1989).

[6]J. Rodriguez-Carvajal, M. T. Fernandez-Diaz, and J. L. Martinez, J. Phys.: Condens. Matter **3**, 3215 (1991).

[7]J. D. Jorgensen, B. Dabrowski, S. Pei, D. G. Hinks, L. Soderholm, B. Morosin, J. E. Schirber, E. L. Venturim, and D. S. Ginley, Phys. Rev. B **38**, 11 337 (1988).

[8]A. C. Larson and R. B. Von Dreele (unpublished).

[9]C. J. Howard, J. Appl. Crystallogr. **15**, 615 (1982); P. Thompson, D. E. Cox, and J. B. Hastings, J. Appl. Crystallogr. **20**, 79 (1987).

[10]C. N. R. Rao, D. J. Buttrey, N. Otsuka, P. Ganguly, H. R. Harrison, C. J. Sandberg, and J. M. Honig, J. Solid State Chem. **51**, 266 (1984).

[11]F. A. Kröger and H. J. Vink, in *Solid State Physics: Advances in Research and Applications,* edited by F. Seitz and D. Turnbull (Academic, New York, 1956), Vol. 3, p. 307.

[12]B. Dabrowski, J. D. Jorgensen, D. G. Hinks, S. Pei, D. R. Richards, H. B. Vanfleet, and D. L. Decker, Physica C **162-164**, 99 (1989).

[13]I. D. Brown, Z. Kristallogr. **199**, 255 (1992).

[14]R. D. Shannon and C. T. Prewitt, Acta Crystallogr. B **25**, 925 (1969).

[15]E. Hecht and A. Zajac, *Optics* (Addison-Wesley, Reading, MA, 1979), p. 359.